



Original article

## Influence of Strain Rate on Metallurgical and Mechanical Properties of Friction Stir Spot Welded Aluminium Joints

\*Danka Labus Zlatanović<sup>1,2</sup>, Jean Pierre Bergmann<sup>1</sup>, Sebastian Baloš<sup>2</sup>, Petar Janjatović<sup>2</sup>,  
 Dragan Rajnović<sup>2</sup>, Leposava Šidjanin<sup>2†</sup>

<sup>1</sup>Department of Production Technology, Technische Universität Ilmenau, 98693 Ilmenau, Germany

<sup>2</sup>Department of Production Engineering, Faculty of Technical Science, University of Novi Sad, 21000 Novi Sad, Serbia.

### ABSTRACT

Nowadays, the substitution of copper with aluminium is widely pursued in order to save weight and material costs, for battery components and wire connectors. Additionally, cost reductions can be further enhanced with effective reduction of energy consumption through efficient manufacturing. Therefore, friction stir spot welding as a solid-state welding technique is a potential choice with low energy demands and high joining performances. However, the joining of aluminium and its alloys with solid-state welding techniques is still a challenging task due to a persistent and chemically stable aluminium oxide layer formed at the sheets prior to the welding, due to the reaction between aluminium and atmospheric oxygen. In this paper, the influence of strain rate induced during friction stir spot welding process on the metallurgical, mechanical and electrical properties of friction stir spot welding of AA 5754-H111 was studied. The strain rate was calculated according to the rotational speed of the tool and the effective (average) radius and depth of the stir zone. It was observed that the specimens welded with a lower strain rate endured a 15 % higher average strain failure load compared to the specimens welded at a higher share rate. The microhardness profiles of the specimens obtained at low strain rates imply strain hardening mechanisms in the weld zone, while the microhardness of specimens welded at high strain rates expressed thermal softening. It was also found that the friction welded sheets, regardless of the strain rate, show increased electrical resistance compared to the base material, however, it decreases with an increase in strain rate. Microstructural analysis reveals a stress-induced metallurgical transformation in the narrow zone around the weld-faying interface.

**Key words:** Friction stir spot welding, Residual oxide defects, Al-Mg alloy, Thermal softening, Dynamic precipitation.

### 1. INTRODUCTION

Automotive and aerospace industry requirements for low-weight components have caused aluminium and its alloys to become key choices in today's manufacturing. Economic motives, competitive market demands and weight reduction, provided the substitution of copper (8.96 g/cm<sup>3</sup>) for aluminium (2.7 g/cm<sup>3</sup>) to gain full attention for battery components, strand-terminal connectors, etc. [1].

Consequently, the challenge of establishing the improved joining technologies for aluminium and its alloys with suitable weld characteristics and lowest energy consumption has emerged [2, 3]. However, the joining of aluminium and its alloys, with solid-state welding techniques is demanding due to the chemically stable oxide layer on the top and at the surface of the sheet before joining, as a consequence of the reaction between aluminium and atmospheric oxygen [4].

\* Corresponding author's.e-mail: danlabus@uns.ac.rs

Published by the University of Novi Sad, Faculty of Technical Sciences, Novi Sad, Serbia.

This is an open access article distributed under the CC BY-NC-ND 4.0 terms and conditions

Friction stir spot welding (FSSW) offers a number of advantages compared to the other welding techniques such as high mechanical properties, small or no distortion of welds, low energy consumption, and no consumable or shielding gas needed [5]. Compared to conventional friction stir spot welding (CFSSW), where a keyhole is left behind, causing a reduction of mechanical properties, probe-less tool friction stir spot welding (PLT-FSSW) was used. During PLT-FSSW, the deformation brought by the tool results in stretch-induced strain in the workpieces causing fragmentation of the brittle oxide layer between the sheets at the weld-faying interface (WFI). As these fragments remain entrapped within WFI, they reduce the homogeneity in the diffusion bonding resulting in non-uniform weld joint quality and becoming nucleation hotspots for joint fracture [10].

Sato et al. [6] first analysed the influence of the oxide layer on the mechanical properties of friction stir welded joints (AA 1050). It was shown that entrapped residual oxides cause kissing bond defects, which are responsible for delamination during bending tests. Due to a different joint geometry during lap joining (FSSW vs. FSW) the residual oxide defects cause the formation of bonding ligaments, which are responsible for the reduction of joining strength [7] Tier et al. [8] studied the influence of rotational speed on the length of bonding ligaments during refill friction stir spot welding. They found that the reduction of rotational speed from 1900 to 900 RPM increases the length of BL. Li et al. [9] studied the effects of rotational speed on the weld quality during RFSSW of 2A12- T4 aluminium alloy. The tensile-shear properties of welds depend on hook geometry and the distribution of bonding ligament. With increasing rotational speed from 900 to 1300 RPM, the bonding ligaments of the weld periphery were more dispersed, and the hardness of the stir zone decreased. Recently Labus Zlatanovic et al. [10, 11] analysed the origins of delamination in multiple sheets of AA 5754 aluminium alloy joined by FSSW. Detailed microscopic characterisation revealed the complex interfacial layer formed because of stress-assisted metallurgical transformation at the intersection of WFI.

In this study, the influence of strain rate caused by different rotational speeds during probe-less friction stir spot welding of AA 5754- H111 on mechanical and electrical properties was studied. Micro- and macroscopic analysis with light and transmission electron microscopy was carried out, together with tensile shear and hardness tests.

## 2. EXPERIMENTAL PART

Specimens used for FSSW were cut from rolled aluminium alloy sheets (5754–H111) to 45 × 110 × 0.3 mm dimensions. The chemical composition and mechanical properties are shown in Table 1. and Table 2, respectively. The four sheets were placed one above another and welded together.

Experimental tests were carried out on a force-controlled EJOWELD C50R FSSW machine with a maximal rotational speed of 9000 RPM, maximum force of 8 kN and

maximum welding time of 5 s. Joining of the sheets was done with a convex pin-less tool, used in previous studies [11], made from H13 (X40CrMoV51) hot-work tool steel. Process parameters are shown in Table 3.

Table 1 Chemical composition of commercial AA 5754 - H111 aluminium alloy

Element	Weight (%)
Si	0.19
Fe	0.24
Cu	0.03
Mn	0.30
Mg	3.10
Cr	0.03
Zn	0.005
Ti	0.014
Al	bal.

Table 2. Mechanical properties of AA 5754 – H111 aluminium alloy quoted by the material supplier

Base material	Min. Yield Strength (MPa)	Tensile Strength (MPa)	Elongation – A50 (%)
AA 5754 – H111	80	190-240	10

Table 3. Process parameters

Rotational speed (RPM)	Penetration depth (mm)	Axial load (kN)	Welding time (s)
1000	0.25 4	4	1.43±0.07
2500			1.07±0.08
4000			0.98±0.04

After the joining, the standard metallographic preparation (grinding and polishing) followed by electrolytic etching with Barker's reagent was performed. The crosssection morphology of the joints was analysed by light microscope Zeiss AxioScope.A, for etched specimens and Zeiss Axio Vert.A1 MAT, for polished specimens with crossed polarised light and sensitive tint.

The weld faying interface was analysed with a 200 kV transmission electron microscope (TEM, Tecnai Osiris, FEI) additionally equipped with a scanning unit (STEM) including a highangle annular dark-field (HAADF, Fischione Co.) detector and energy dispersive X-ray spectrometer (EDX, Super-X system with 4 Bruker silicon drift detectors, Thermo Fisher Co.). Electrical properties were determined according to the explanation in previous work [11].

Microhardness test was done by using standard Vickers microhardness test with Struers DuraScan 70 machine with 0.1 kg loading and distance between indentations of 0.33 mm. A Hegewald & Peschke Inspect Retrofit universal tensile testing machine with a maximal load of 20 kN was used to test tensile shear specimens. The testing speed was set to be 10 mm/min, and the test set-up was explained in

previous work [11]. Testing was performed on all three weld-faying interfaces.

### 3. RESULTS AND DISCUSSION

#### 3.1 Coefficient of Friction and strain Rate Calculations

The variation in the coefficient of friction (CoF) was calculated by using Equation (1) [12]. In this paper, the CoF was calculated by using axial force and torque data generated from the FSSW equipment. Although the axial force was constant at the beginning of the process, monitored axial force, which slightly differs from fixed, was used in the calculation to obtain a data with higher accuracy contact. Also, the radius of the tool calculated according to equation (2) used for the estimation of the CoF changed during the process from 0 to 3.34 mm. Therefore, in CoF equation time-dependent torque, axial load and contact radius were used, and results are also presented as time depended diagrams.

$$\mu(t) = \frac{\tau}{\sigma_n} = \frac{2T(t)}{F_N(t)r(t)} \quad (1)$$

$T$  - shear stress (MPa)

$\sigma_n$  - normal stress (MPa)

$T(t)$  - torque (N·mm)

$F_N(t)$  - axial load (N)

$r(t)$  - tool contact radius [mm]. It can be calculated from the following equation:

$$r(t) = \frac{\sqrt{4R^2 - (2R - 2h)^2}}{2} \quad (2)$$

where  $R$  is the fixed tool radius (mm),  $h(t)$  is the axial displacement of the tool (penetration depth) (mm) [13].

The CoF vary from 0.6 to 2 as shown in Fig. 1. In a specimen welded with 1000 RPM where the CoF increases with welding time, the strain hardening overcomes thermal softening. The frictional properties are governed by the properties of the strain-hardened workpiece. In specimens where CoF increases shortly at the beginning and then decreases with the increase of welding time, thermal softening overcame strain hardening after reaching the highest value of the CoF. Between them is a specimen welded at 2500 RPM where CoF swings without significant increase or decrease, making the strain hardening and thermal softening almost equally influential in the evolution of CoF.

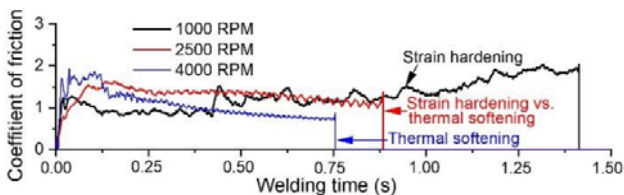


Fig. 1 Variation in the coefficient of friction over dwell time

Kumar et al. [14] and Farhat et al. [15] reported, that during the initial interaction between the tool and workpiece, friction is driven by the grains from base material. As the interaction increases, the material in the sub and surface deforms and due to strain hardening of the material competing against thermal softening the hardness increases. Thus, the two opposite driving forces are working against each other to impose the conditions and microstructure of the workpiece at the end of the process. Materials like aluminium-magnesium alloys tend to express Portevin-Le Chatelier (PLC) effect during inhomogeneous plastic deformation. Under conditions of local increase of the strain rate above a certain limit, softening of the material locally occurs. Next, the formula proposed by Chang et al. [16] was used to perform calculations for estimating the applied strain rate as a function of rotational speed.

$$\dot{\varepsilon} = \frac{2\pi R_m r_e}{L_e} \quad (3)$$

where  $r_e$  and  $L_e$  are the effective (average) radius and depth of the stir zone measured with the ImageJ software from cross-sections of etched specimens. Chang et al. [16] estimated the average material flow  $R_m$  to be half of the tool rotation speed. The results of strain rate calculations are presented in Table 4. Together with process temperatures.

Table 1 Maximal temperature and strain rate obtained from eq. (3)

Rotational speed (RPM)	Weight (%)	Strain rate (s <sup>-1</sup> )
1000	101±5	175
2500	135±4	441
4000	156±10	612

Values in table show that during FSSW, the strain rate increases with rotational speed and maximal temperature. According to stresscycle time plots, CoF vs. time plots and hardness measurements, it can be concluded that strain hardening is more pronounced at strain rates lower than 441 s<sup>-1</sup> and low process temperature and thermal softening is more pronounced at strain rates >441 s<sup>-1</sup> followed by higher process temperature.

#### 3.2 Macro and Microstructural Evaluation

Cross-sections of polished and etched specimens obtained at rotational speeds 1000, 2500 and 4000 RPM are shown in Fig.2. The polished specimens do not reveal delamination or any other defects in the welded specimen. A uniform weld zone without a visible weld interface can be observed. However, after etching of the specimen, bonding ligaments at all three WFI become visible.

The variations in the grain size are presented in Fig. 3, respectively. It was observed that the low RPM (low strain rate < 441 s<sup>-1</sup>) leads to small grain sizes while high RPM (strain rate > 441 s<sup>-1</sup>) causes grains to be coarse. Jata et al. [17] proposed that the main grain refinement mechanism during FSSW is continuous dynamic recrystallization

(CDRX). This process is driven by temperature and strain rate. Furthermore, the interaction between precipitates and solute atoms with dislocations has a high influence.

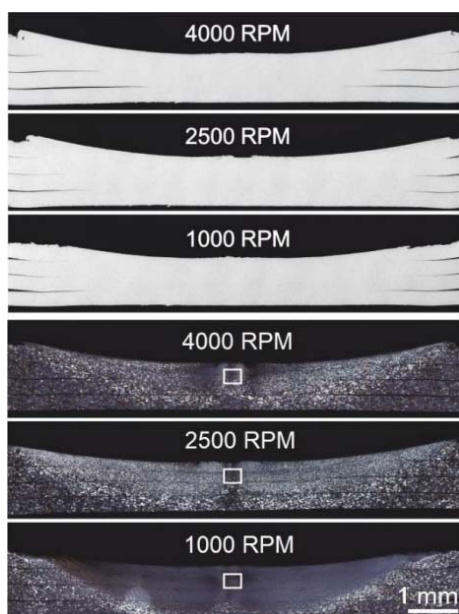


Fig. 2 Polished and etched cross-section views of the welded joints (4000, 2500 and 1000 RPM)

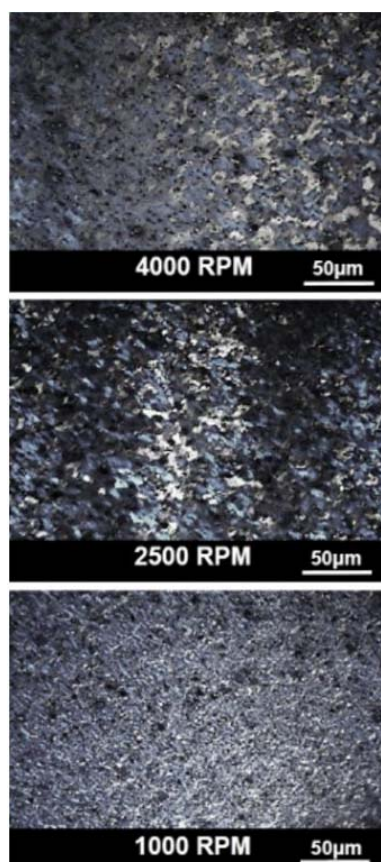


Fig. 3 Micrographs of specimens welded at 4000, 2500 and 1000 RPM (taken in the area of the white square in Fig. 2)

The STEM bright-field image of the weld faying interface between the last two sheets, including the recrystallized stir

zone, is presented in Figure 4. The image shows the presence of ultrafine globular precipitates in grain boundaries of WFI, originating from dynamic precipitation [10]. A high number of precipitates can be seen at the boundary between the recrystallised stir zone and the weld faying interface. Polygonal grains in recrystallised stir zone and fibrous grains in weld faying interface, both contain randomly dispersed globular Al<sub>6</sub>(FeMn) precipitates which are typical in an AA 5754 alloy [10]. At the centre of the weld faying interface, which is the junction of the two sheets, the disturbed oxide layer combined with nano and micro pits can be found. The aluminium oxide layer acted as a barrier to prevent metal atoms from diffusing from one sheet to form stable bonds with another sheet.

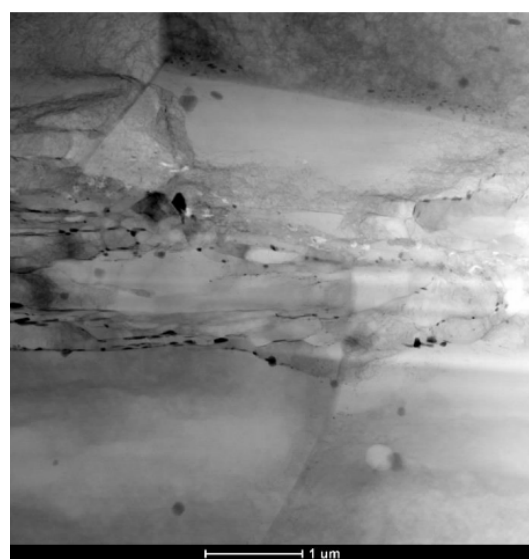


Fig. 4 Scanning transmission electron micrographs of third weld faying interface of specimen welded at 1000 RPM

EDX analysis was used to determine chemical composition of the oxide and shown in Figure 5. At the weld faying interface, the disturbed oxide layer combined with nano and micro pits is present. The disturbed oxide layer prevents metal atoms from diffusing from one sheet to another. During solid-state bonding, usually the oxide layer is about 5–10 nm thick Al<sub>2</sub>O<sub>3</sub>, however, when alloy contains active elements such as magnesium, amorphous Al<sub>2</sub>O<sub>3</sub> can react with Mg to form crystalline MgO [18]. Shen et al. [19] found that the welding interface of AA 6061-T4 obtained by the conventional FSSW contained an array of discontinuous oxide particles causing poor welding. Furthermore, Reilly et al. [20] also proposed that the penetration of the tool into the weld zone stretches the weld interface as well as brittle oxide. Thus, diffusion occurs between oxide fragments.

### 3.3 Mechanical Properties

To understand the effect of size and composition of weld faying interface on the mechanical properties of the weld, microhardness and shear-tensile tests were done. The effect of strain hardening at low RPMs was verified by

Vickers hardness maps presented in Fig.6, revealing that the microhardness on the surface was highest in the welded zone for specimens welded at low rotational speeds. Therefore, in specimens welded at 1000 RPM, the strain hardening mechanism dominates over thermal softening, and conversely, in specimens welded at 2500 and 4000 RPM, thermal softening was more pronounced.

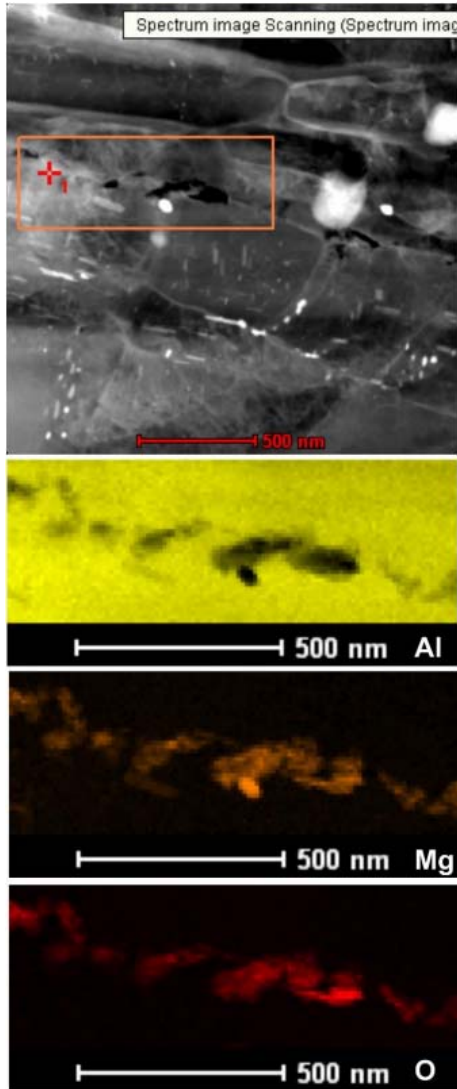


Fig. 5 High-angle annular dark-field scanning transmission electron microscope image of the boundary between weld faying interface and recrystallised stir zone with corresponding energy dispersive X-ray spectroscopy (STEM/EDX) elemental mappings of the area marked in overview

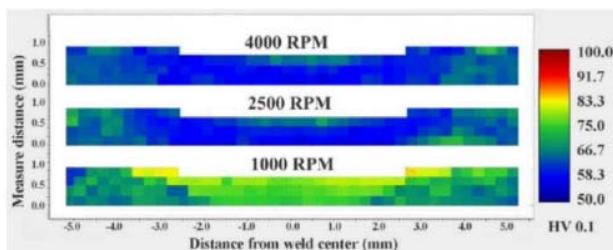


Fig. 6 Vickers microhardness maps at the crosssection of specimens processed at rotational speeds 1000, 2500 and 4000 RPM

Thermal softening of the stir zone in the specimens welded at 4500 RPM causes shear failure load to reduce as shown in Fig.7. On the other hand, the strain hardening of the stir zone in the specimens welded at 1000 RPM significantly improves the mechanical properties of the weld which is supported by microhardness maps.

The rotational speed also influences the size of the welded surface which can be seen on polished specimens in Figure 2. The difference in the size of the welded surface is most pronounced in the I and III weld faying interface, while the II weld faying interface in all specimens are approximately the same. However, even though the size of the welded surface in the I weld faying interface for the specimen welded at 4000 RPM is significantly higher compared to that of 1000 RPM, the shear failure load was almost the same (Fig. 7.). This was caused by the higher mechanical properties of the strain-hardened stir zone of the weld obtained at 1000 RPM compared to the thermal softened stir zone of the specimen welded at 4000 RPM. Furthermore, the welded surface of the I weld faying interface is larger than that of the II weld faying interface, yet the shear failure load is higher in II. For that was responsible significant thinning of the first sheet due to the penetration of the tool. The size of the III weld faying interface was the smallest of all three, which caused the shear load to be the lowest as well.

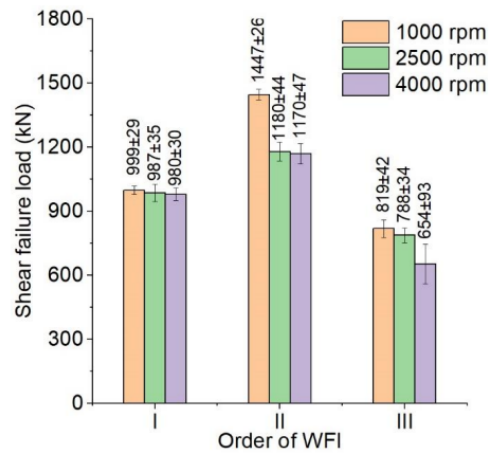


Fig. 7 Influence of rotational speed and order of WFI on the shear failure load

The variation in specific electrical resistance of the base material and specimens welded at 1000 and 4000 RPM is presented in Table 5. The specimens welded at 1000 RPM showed higher specific electrical resistance, followed by the specimen welded at 4000 RPM. The lowest specific resistance was for the base material. In the specimens welded at 1000 RPM, strain hardening is leading, and this causes the dislocations accumulation.

Table 1 Specific electrical resistance

Specimen	Specific electrical resistance (mΩ·mm)
Base material	42.9±0.8
1000 RPM	77.0±2.3
4500 RPM	52.0±1.8

The increase in dislocation density causes an increase in the specific resistance. In the specimen welded at 1000 RPM, there were three faying interface regions with a large number of intermetallics. Furthermore, there is also an oxide layer in the middle of every WFI with a very high electrical resistance combined with nano pits. All those facts combined to cause the electrical resistance of the weld to vary, and this influence in weld quality.

#### 4. CONCLUSION

Friction stir spot welding (FSSW) is becoming promising technology for welding battery components, connectors, standard-thermal and terminals. However, one of the biggest issues driven by this technique is to provide quality weld joints with low electrical resistance, which is an important requirement of the electrical industry. The conclusions drawn from this research can be summarised as follows:

- (i) The coefficient of friction (CoF) was found to vary with the rotational speed. At low rotational speeds, as a strain hardening effect prevails, the CoF increased up to the end of the process. However, in specimens welded at higher rotational speeds thermal softening caused a decrease of CoF upon the welding time.
- (ii) The origins of the delamination between weld sheets were observed to be due to the metallurgical transformations in the narrow region at the weld interface. This narrow zone was composed of precipitates of Al<sub>6</sub>(FeMn) and a weld faying interface, which had significantly smaller fibrous grains with a high volume of precipitates of Al<sub>3</sub>Mg<sub>2</sub>. Additionally, within the weld faying interface, sites of nano- and micropits combined with a rich presence of MgO were found to be present as well.
- (iii) Shear strength and microhardness were highest in specimens obtained at 1000 RPM. The II weld faying interface expressed the highest shear strength in all specimens, while the III weld faying interface showed the lowest. In specimens welded at 1000 RPM, microhardness increased compared to the base material due to strain hardening, whereas in specimens welded at 4000 RPM, the microhardness of the stir zone decreased below the base material due to a predominant thermal softening mechanism.
- (iv) It was noted that the electrical resistance of the weld joints depends on the rotational speed. Although the electrical resistance of the welds was found to be higher in all cases compared to the base material, concerning the base material, it increases for low rotation speed more than for higher rotation speed.

#### ACKNOWLEDGEMENT

The authors gratefully acknowledge research support by the project entitled “Advanced materials, joining and allied

technologies” at the Department of Production Engineering, Faculty of Technical Sciences Novi Sad, Serbia.

#### REFERENCES

- [1] Pryor L, Schlobohm R, Brownell B. A. Comparison of Aluminum Vs. Copper As Used in Electrical Equipment. *Corrosion*, 2008, p. 1–7.
- [2] Regensburg A, Petzoldt F, Bess T, Bergmann JP. Liquid interlayer formation during friction stir spot welding of aluminium / copper. *Weld World* 2018; 63:117–25.
- [3] Labus Zlatanovic D. Friction stir spot welding of ultrathin sheets made of aluminium – magnesium alloy, PhD thesis. University of Novi Sad, 2020.
- [4] Labus Zlatanovic D, Bergmann JP, Balos S, Hildebrand J, Bojanic-Sejat M, Goel S. Effect of surface oxide layers in solid-state welding of aluminium alloys – review. *Sci Technol Weld Join* ISSN 2023:1–21. <https://doi.org/10.1080/13621718.2023.2165603>.
- [5] Sun Y, Morisada Y, Fujii H, Tsuji N. Ultrafine grained structure and improved mechanical properties of low-temperature friction stir spot welded 6061-T6 Al alloys. *Mater Charact* 2018; 135:124–33. <https://doi.org/10.1016/j.matchar.2017.11.033>.
- [6] Sato YS, Takauchi H, Park SHC, Kokawa H. Characteristics of the kissing-bond in friction stir welded Al alloy 1050. *Mater Sci Eng A* 2005; 405:333–8. <https://doi.org/10.1016/j.msea.2005.06.008>.
- [7] Sarkar R, Pal TK, Shome M. Material flow and intermixing during friction stir spot welding of steel. *J Mater Process Technol* 2016; 227:96–109. <https://doi.org/10.1016/j.jmatprotec.2015.08.006>.
- [8] Tier MD, Rosendo TS, Dos Santos JF, Huber N, Mazzaferro JA, Mazzaferro CP, et al. The influence of refill FSSW parameters on the microstructure and shear strength of 5042 aluminium welds. *J Mater Process Technol* 2013; 213:997–1005. <https://doi.org/10.1016/j.jmatprotec.2012.12.009>.
- [9] Li G, Zhou L, Luo L, Wu X, Guo N. Microstructural evolution and mechanical properties of refill friction stir spot welded Al clad 2A12-T4 aluminum alloy. *J Mater Res Technol* 2019; 8:4115–29. <https://doi.org/10.1016/j.jmrt.2019.07.021>.
- [10] Labus Zlatanovic D, Balos S, Bergmann JP, Rasche S, Zavašnik J, Panchal V, et al. In-depth microscopic characterisation of the weld faying interface revealing stress-induced metallurgical transformations during friction stir spot welding. *Int J Mach Tools Manuf* 2021; 164:103716. <https://doi.org/10.1016/j.ijmactools.2021.103716>.
- [11] Labus Zlatanovic D, Bergmann JP, Balos S, Gräzel M, Pejic D, Sovilj P, et al. Influence of rotational speed on the electrical and mechanical properties of the friction stir spot welded aluminium alloy sheets.

- Weld World 2022. <https://doi.org/10.1007/s40194-022-01267-8>.
- [12] Kalpakijan S. *Manufacturing Processes for Engineering Materials*. Addison Wesley Publishing Company; 1991.
- [13] Labus Zlatanovic D, Baloš S, Bergmann JP, Rasche S, Pecanac M, Goel S. Influence of Tool Geometry and Process Parameters on the Properties of Friction Stir Spot Welded Multiple (AA 5754 H111) Aluminium Sheets. *Materials (Basel)* 2021; 14. <https://doi.org/https://doi.org/10.3390/ma14051157>.
- [14] Kumar K, Kalyan C, Kailas S V, Srivatsan TS. An Investigation of Friction During Friction Stir Welding of Metallic Materials. *Mater Manuf Process* 2009; 24:438–45. <https://doi.org/10.1080/10426910802714340>.
- [15] Farhat ZN, Ding Y, Northwood DO, Alpas AT. Effect of grain size on friction and wear of nanocrystalline aluminum. *Mater Sci Eng A*. 1996; 206:302–13.
- [16] Chang CI, Lee CJ, Huang JC. Relationship between grain size and Zener-Holloman parameter during friction stir processing in AZ31 Mg alloys. *Scr Mater* 2004; 51:509–14. <https://doi.org/10.1016/j.scriptamat.2004.05.043>.
- [17] Jata K, Semiatin S. Continuous dynamic recrystallization during friction stir welding of high strength aluminum alloys. *Scr Mater* 2000; 43:743–9. [https://doi.org/10.1016/S1359-6462\(00\)00480-2](https://doi.org/10.1016/S1359-6462(00)00480-2).
- [18] Shirzadi AA, Assadi H, Wallach ER. Interface evolution and bond strength when diffusion bonding materials with stable oxide films. *Surf Interface Anal* 2001; 31:609–18. <https://doi.org/10.1002/sia.1088>.
- [19] Shen Z, Yang X, Zhang Z, Cui L, Yin Y. Mechanical properties and failure mechanisms of friction stir spot welds of AA 6061-T4 sheets. *Mater Des* 2013; 49:181–91. <https://doi.org/10.1016/j.matdes.2013.01.066>.
- [20] Reilly A, Shercliff H, Chen Y, Prangnell P. Modelling and visualisation of material flow in friction stir spot welding. *J Mater Process Technol* 2015; 225:473–84. <https://doi.org/10.1016/j.jmatprotec.2015.06.021>.

#### NOTE

This paper is based on the paper presented at 39th International Conference on production Engineering of Serbia – ICPEs 2023, organized by University of Novi Sad, Faculty of technical sciences, 6 - 27. October 2023, Novi Sad, Serbia.